PROCEEDINGS OF SCIENCE

A model independent parametrization of the optical properties of the refrozen IceCube drill holes

The IceCube Collaboration

(a complete list of authors can be found at the end of the proceedings)

E-mail: philipp.eller@tum.de, martin.rongen@fau.de

The IceCube Neutrino Observatory deployed 5160 digital optical modules (DOMs) in a cubic kilometer of deep, glacial ice below the geographic South Pole, recording the Cherenkov light of passing charged particles. While the optical properties of the undisturbed ice are nowadays well understood, the properties of the refrozen drill holes still pose a challenge. From camera observations, we expect a central, strongly scattering column shadowing a part of the DOMs' sensitive area. In MC simulation, this effect is commonly modeled as a modification to the DOMs' angular acceptance curve, reducing the forward sensitivity of the DOMs. The associated uncertainty is a dominant detector systematic for neutrino oscillation studies as well as high-energy cascade reconstructions. Over the years, several measurements and fits of the drill holes' optical properties and of the angular acceptance curve have been proposed, some of which are in tension. Here, we present a principle component analysis, which allows us to interpolate between all suggested scenarios, and thus provide a complete systematic variation within a unified framework at analysis level.

Corresponding authors: Philipp Eller[1*], Martin Rongen[2]

[1] *Technical University of Munich, TUM School of Natural Sciences, Physics Department, 85747 Garching, Germany*

[2] *Erlangen Centre for Astroparticle Physics, Friedrich-Alexander Universität Erlangen-Nürnberg*

[*] Presenter

The 38th International Cosmic Ray Conference (ICRC2023)
26 July – 3 August, 2023
Nagoya, Japan

© Copyright owned by the author(s) under the terms of the Creative Commons Attribution-NonCommercial-NoDerivatives 4.0 International License (CC BY-NC-ND 4.0).

PoS(ICRC2023)1034

1. Introduction

The IceCube Neutrino Observatory [1] is located in the deep glacial ice below the geographic South Pole. It is comprised of 5160 *Digital Optical Modules (DOMs)* each incorporating a 10-inch, downward facing photomultiplier tube to detect Cherenkov light produced by relativistic charged particles traversing the detector. The DOMs were deployed along so called *strings* in 86 drill holes of ~60 cm diameter at depths spanning between 1450 m and 2450 m. While the dominant part of the propagation of Cherenkov photons from their emission to an eventual detection happens in the exceptionally clear, bulk glacial ice, each photon detected by a DOM also had to propagate through the refrozen water in a drill hole, the so called *hole ice*. This hole ice is modeled as a variation of the optical acceptance of DOMs as a function of the photon incident zenith angle.

While the calibration and modeling of the optical properties of the bulk glacial ice has continuously improved over the years [2–4], the optical properties of the hole ice are less well understood. Years ago the uncertainties in most IceCube analyses were dominated by statistics, today for example the DeepCore oscillation analyses [5–7] are limited by uncertainties of detector effects such as bulk ice properties and the overall optical efficiency of the modules, but also especially the angular acceptance of modules that is discussed here. Since optical effects have to be modeled in simulation by altering the photon propagation and acceptance, incorporating such effects in analyses as nuisance parameters is computationally costly. The usual approach is to either build interpolating functions between discrete simulation sets (e.g. [8]) or using random sampling of simulation configurations (e.g. [9]).

We lay out three properties a good model should fulfill:

1. Provide enough flexibility to cover a large enough range of scenarios to be able to describe the data
2. Use as few parameters as possible to reduce computational burden on simulation and inference
3. Define a specified range of parameter values to inform the simulation to cover a useful space of possibilities

These points are addressed in this work, and documented in the following sections: Section 2 summarizes several measurements and fits of the drill holes' optical properties and of the angular acceptance curve that have been proposed in the past. In Sec. 3 we introduce our new two-parameter model that allows us to interpolate between all suggested scenarios, and thus provide a complete systematic variation within a unified framework at analysis level. The parameters of this model are fitted to LED calibration data in Sec. 4. Finally a comparative overview over input models, the results from the LED fit as well as results from nuisance parameter fits in physics analyses using the described model is provided.

2. Previous Models

Direct visual evidence for the existence and properties of the refrozen drill columns has been provided by a pair of cameras situated at the bottom of a string [1]. As seen in Figure 1, the outer regions of the drill hole are exceptionally clear, but the inner ~16 cm appear diffuse white, as would

PoS(ICRC2023)1034

Figure 1: Sweden Camera image of the lower camera looking straight up at the upper camera, with the hole ice fully developed in the right half of the image. [10]

be expected from strong scattering on air bubbles. This concurs with a model where the water filled holes freeze cylindrically inwards with impurities, including air bubbles, being continuously pushed ahead of the freezing boundary until they precipitate out in high concentration in the center of the hole. This feature is commonly denoted the *bubble column*.

In simulation the bubble column can be included directly by physically modeling the photocathode extend as well as an extended bubble column with assumed diameter, scattering properties and position with respect to each DOM. This very precise approach has recently been pursued successfully in [11] and [12], but is computationally expensive. Thus, the effect induced by the bubble column is instead commonly modeled via an angular acceptance curve. In this approximation the landing position of a photon on the surface of a DOM is disregarded when evaluating the detection probability in simulation and instead the efficiency is only based on the cosine of the zenith angle of the photon direction at the time of impact on the module ($\cos\eta$).

Approximating a DOM to be homogeneously sensitive on its entire lower hemisphere, its bare relative detection efficiency (y) is then given as $y_{\text{ideal}} = 0.5 \cdot (1 + \cos\eta)$. The angular acceptance curve resulting from a precise knowledge of the DOM's hardware properties [2, 11] is denoted *Lab* in Figure 2. Incorporating the effect of the hole ice into the angular acceptance generally decreases the forward acceptance at $\cos\eta = 1$, as the hole ice effectively shadows off a part of the photocathode.

The earliest, but still commonly used models, were derived for the IceCube predecessor AMANDA [11, 13]. Here, lacking the later visual camera evidence, it was assumed that the entire ~60 cm drill hole would have degraded optical properties with geometric scattering length in the range between 50 cm and 100 cm.

Within IceCube the optical properties are most commonly deduced from fits to LED calibration data, which have little direct sensitivity to the forward acceptance. For this reason, previous fits [11]

PoS(ICRC2023)1034

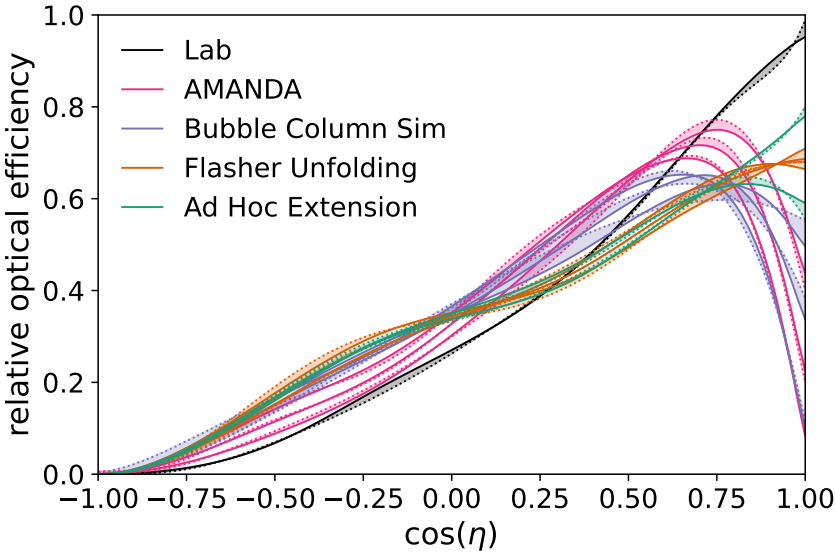

Figure 2: DOM angular acceptance curves from previous modeling attempts, used as input for the Unified Model described in this work. The acceptances are shown as functions of the PMT incident angle η, where $\cos\eta = 1$ means photons coming head-on to the photocathode area. *Lab* denotes the DOM characteristics without hole ice. *AMANDA* refers to measurements performed by a laser system in the IceCube predecessor AMANDA. *Flasher Unfolding* refers to a constrained unfolding using IceCube LED calibration data. *Ad Hoc Extension* is a parametric extension of this model used in previous neutrino oscillation fit. And *Bubble column Simulation* is a set of curves derived from a first principle simulation of photon propagation through allowed hole ice configurations. In each case the dotted line shows the original input model, while the solid line shows the closest representation of this input within the two parameters of the Unified model.

used the following functional form for the angular acceptance

$$y = 0.34(1 + 1.5\cos\eta - \cos^3\eta/2) + p \cdot \cos\eta(\cos^2\eta - 1)^3. \tag{1}$$

It is constrained to a reasonable value for the forward acceptance, roughly shading of 30% of the photocathode area, and the free parameter p only changes the shape for intermediate values of $\cos\eta$.

Yet, as the forward acceptance is of primary importance as a systematic uncertainty for analyses, this constraint was lifted in an ad-hoc parametric extension, which allows for an arbitrary forward acceptance through a second parameter [14]:

$$y = 0.34(1 + 1.5\cos\eta - \cos^3\eta/2) + p \cdot \cos\eta(\cos^2\eta - 1)^3 + p2 \cdot \exp(10(\cos\eta - 1.2)). \tag{2}$$

While the previously mentioned direct simulation of photon propagation through a bubble column is conceptually different from the angular acceptance parametrization, the hole ice properties (size and scattering length) deduced there can also be translated into angular acceptance curves assuming the bubble column to be centered on all DOMs. These curves, with assumed diameters ranging between 18 cm and 54 cm and effective scattering lengths ranging between 14 cm and 125 cm respectively are denoted as *Bubble Column Simulation* in the following. The allowed parameters were derived in [11] and have since been superseded by [12]. As the update primarily affected the per-DOM positions of the bubble column, but not the size and scattering length, the curves are still assumed to represent the best knowledge at present.

PoS(ICRC2023)1034

3. Unified Model

The aim of the unified model is to define a parameterization with as few parameters as possible that can approximate all existing angular acceptance curves as discussed in the previous section and shown in Fig. 3, as well as interpolate between those and extrapolate outside. Note that the ad-hoc model presented in the previous section is also based on just two parameters, but it does not offer enough flexibility to approximate other models and variations of its acceptance curves are constrained to a small region.

We begin by approximating the existing curves using an interpolating B-spline of order $k = 3$ (cubic). Seven support points for the spline are defined at:

$$x = \cos\eta = (-1, -0.5, -0.2, 0.35, 0.65, 0.95, 1.05), \tag{3}$$

where the last point extends outside the physically allowed region. These values have been heuristically determined to work well. The corresponding points in y (= relative optical efficiency) are free parameters except for the points at $x = -1$ where the value is fixed to $y = 0$, since photons arriving from behind the PMT can not be detected. Furthermore, derivatives are fixed to zero at either end of the spline. This means that with with the six parameters (degrees of freedom) constituting y we define B-splines that make up angular acceptance curves. In a fit to the original twelve curves discussed in the previous section, the best values for y are determined by minimizing the mean-squared error between the original curves and their B-spline approximations. This means that all models can be described by a matrix $\mathbf{S}$ of (12×6) values.

In order to facilitate the usage of the new model in physics analyses, we want to reduce the dimensionality as much as possible, to end up with a minimal number of nuisance parameters to vary in simulation and inference. We apply a singular value decomposition (SVD) to the matrix $\mathbf{S}$ to express it in the form $\mathbf{U\Sigma V}^*$. This can then be interpreted as a set of six principal components p per calibration curve collected in the matrix $\mathbf{U\Sigma}$ and six principal directions arranged in matrix $\mathbf{V}$.

Reducing the number of principal components and accordingly the components of the direction vectors is known as a principal component analysis (PCA) allowing to reduce dimensionality. It turns out that by only using the first two components, henceforth referred to as p_0 and p_1, is sufficient to reconstruct all input curves to a precision of $< 5\%$. The fitted principal directions are given below:

$$\mathbf{V}^* = \begin{pmatrix} -0.0054533 & 0.0165525 & -0.136688 & -0.0782252 & 0.5139002 & 0.8430896 \\ -0.4508718 & -0.5179942 & 0.2407660 & 0.6061325 & 0.3092565 & -0.0859777 \end{pmatrix} \tag{4}$$

and the original points y needed for the B-spline can then be reconstructed as:

$$y - \langle y \rangle = (p_0, p_1) \cdot \mathbf{V}^* \tag{5}$$

where the mean that was subtracted in the decomposition is equal to:

$$\langle y \rangle = (0.14623077, 0.26576604, 0.4832101, 0.63038745, 0.57494938, 0.48991044). \tag{6}$$

Having a vector y at hand given a choice of parameters (p_0, p_1) then allows to construct the B-spline describing the angular acceptance curve. This curve is then in further processing steps

PoS(ICRC2023)1034

clipped to be greater or equal to zero everywhere, and then normalized to equal area under the curve such that all curves reflect the same total efficiency.

In summary, the outlined procedure defines a two-parameter unified model that can generate an angular acceptance curve for a choice of input parameters (p_0, p_1), and is able to approximate all existing calibration curves as discussed in the previous section to an accuracy of $< 5\%$.

Figure 3 shows some example curves for varying inputs of p_0 and p_1, respectively. It can be noted that the first component p_0 results in a modulation of only the head-on region of the PMT ($\cos\eta \gtrapprox 0$), while component p_1 affects mostly the shape around the waist of the PMT. Figure 2 shows the fidelity of the 2-parameter approximation of the unified model compared to the initial calibration curves used as inputs. The maximum range of the parameters that produces sensible curves is roughly $-2 < p_0 < 1$ and $-0.2 < p_1 < 0.2$.

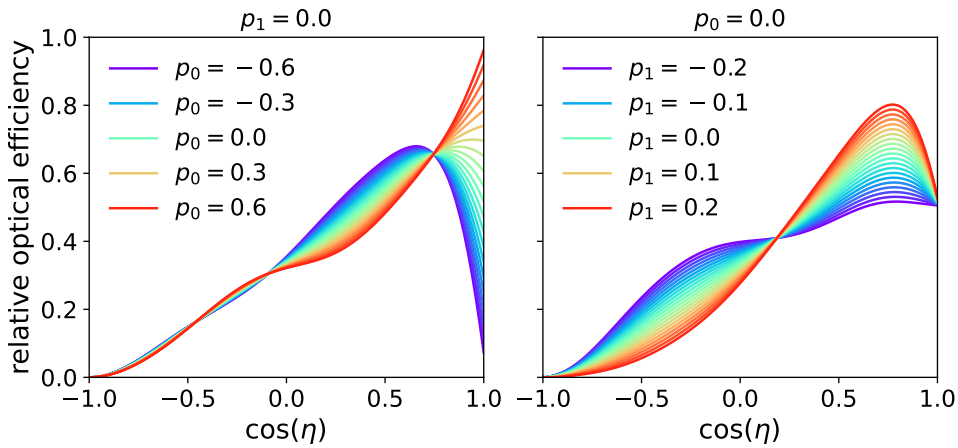

Figure 3: Example angular acceptance curves, resulting from variations of the p_0 and p_1 parameters of the Unified model. p_0 primarily suppresses the forward-acceptance and thus models the fraction of shadowed photocathode area, while p_1 primarily modifies the slope and thus isotropy of detection.

4. Flasher fit

While the parametrization has been derived from plausible models resulting from fits to muon and LED calibration data, its parameters can also be fitted directly. This in particular allows to constrain a sensible region for large-scale simulations to be conducted.

To this end a fit to LED calibration data, selecting data from DOMs on six standard IceCube strings surrounding DeepCore and at depth exceeding 2100 m, each flashing their 12 LEDs [15] in sequence, has been performed. The fit follows the methodology as described in [2, 11], comparing the arrival time distributions in data to photon propagation simulation [16], with only the hole ice parameters being varied in simulation. All other aspects and parameter values of the ice optical modeling are taken from the so-called Spice3.2 ice model [11].

Figure 4 shows the resulting likelihood space, with each grid cell being intensity coded according to the distance of the likelihood value of one simulated hole ice realization from the best-fit realization. The employed likelihood (see [17]) accounts for the vastly smaller photon statistics in

PoS(ICRC2023)1034

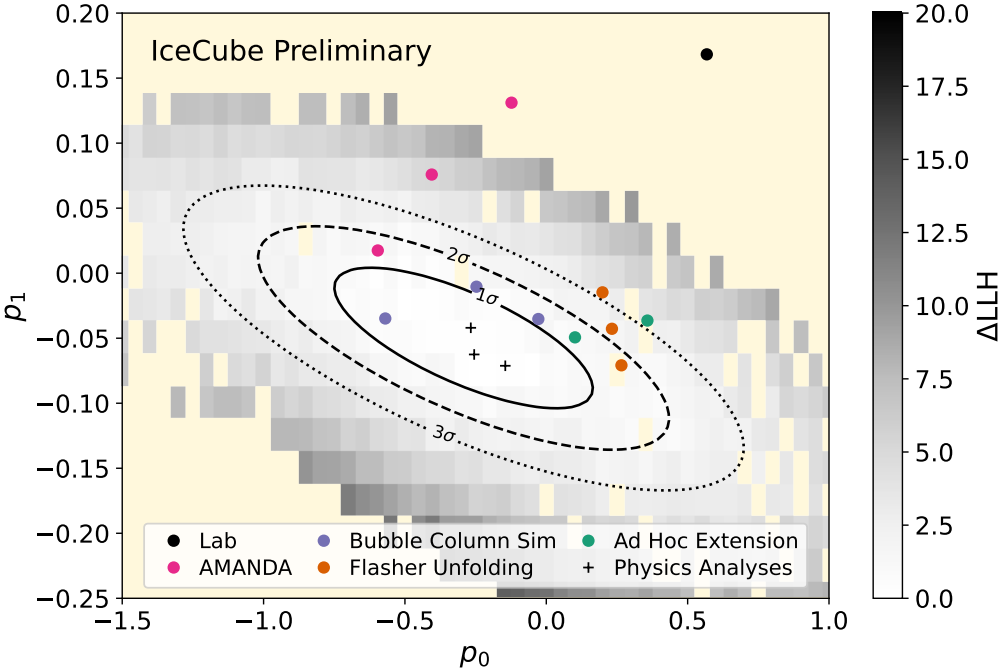

Figure 4: p_0-p_1-parameter landscape of the Unified Model. Colored circles denote the parameter values of the input models used to build the parametrization. The intensity coded grid cells show the delta likelihood value of a flasher fit for the given simulated hole ice realization. The fit was performed using 120 light emitting DOMs surrounding DeepCore at depths greater then 2100 m. The contours denote the statistical error only and are dominated by the simulation statistics. The black crosses denote the preferred values as resulting from nuisance parameter fits in several low- and high-energy physics analyses.

simulation compared to the experimental data. This induces fluctuations of the likelihood values compared to the expected paraboloid. The statistics-only uncertainty contours as shown account for this fluctuation by fitting a polynomial. As the likelihood does not conform to Wilk's Theorem the ΔLLH values for a given coverage have been calculated from the residuals around this polynomial. The contour sizes primarily reflect the employed simulation statistics, but are representative of the sensitivity of the analysis as a whole. The impact of other systematic detector uncertainties (such as the bulk ice modeling) on the preferred hole ice parameters has not been evaluated in this context, as it would require equivalent fits and thus vastly more simulation.

5. Results & Discussion

Figure 4 shows the values (black crosses) of the maximum likelihood estimators for p_0 and p_1 in three recent IceCube physics analyses that use our model. Interestingly, these values coincide with the minimum of the fit to flasher data, drawing a consistent picture. The fit to flasher data also can make some statements on previously used models, and strongly disfavors the scenario of absence of hole ice, i.e. no altered optical properties in the refrozen drill holes corresponding to the "Lab" curve. Furthermore, the AMANDA models do not seem to be able to correctly describe the IceCube angular acceptance. The previous attempts using simple parametrizations ("Flasher

PoS(ICRC2023)1034

unfolding" and its "Ad Hoc Extension") are also disfavored, albeit at a milder level. The only compatible scenarios seem to be the those derived from the direct simulation of photon propagation in the bubble column termed "Bubble column simulation" above.

Another important aspect is the range of useful parameters, that can also be read off from Fig. 4. For a simple rectangular box, we propose the range of $-1 < p_0 < 0.4$ and $-0.14 < p_1 < 0.04$ roughly covering the 2σ contour. Since the likelihood exhibits a negative correlation coefficient of $\rho = -0.72$ a range of simulations more closely following the contour shape is recommended.

The IceCube Upgrade [18] will, among many more optical sensors, also deploy several new calibration hardware. The Precision optical Calibration Module (POCAM) [19, 20], for example, will allow to collect new calibration data of unprecedented quality. This data is expected to allow us to better understand our detector, including the hole ice and associated angular acceptance.

References

[1] **IceCube** Collaboration *Nucl. Instr. Meth. Phys. Res. A* **601** no. 3, (2009) 294 – 316.

[2] **IceCube** Collaboration *Nucl. Instr. Meth. Phys. Res. A* **711** (May, 2013) 73–89.

[3] **IceCube** Collaboration *PoS* **ICRC2013** (2013) 0580. arXiv:1309.7010.

[4] **IceCube** Collaboration *The Cryosphere Discussions* **2022** (2022) 1–48.

[5] **IceCube** Collaboration, M. G. Aartsen *et al.* *Phys. Rev. Lett.* **120** no. 7, (2018) 071801.

[6] **IceCube** Collaboration, M. G. Aartsen *et al.* *Phys. Rev. D* **99** no. 3, (2019) 032007.

[7] **IceCube** Collaboration, R. Abbasi *et al.* arXiv:2304.12236.

[8] L. Fischer *et al.* arXiv:2305.02257.

[9] **IceCube** Collaboration, M. G. Aartsen *et al.* *JCAP* **10** (2019) 048.

[10] P. O. Hulth. https://indico.fysik.su.se/event/3930/contributions/4803/contribution.pdf.

[11] M. Rongen *Dissertation* **RWTH Aachen University** (2019) 2019.

[12] **IceCube** Collaboration *PoS* **ICRC2021** (2021) 1023.

[13] A. Karle and K. Woschnagg. AMANDA internal report.

[14] **IceCube** Collaboration *Phys. Rev. Lett.* **120** (Feb, 2018) 071801.

[15] **IceCube** Collaboration *Journal of Instrumentation* **12** no. 03, (Mar, 2017) P03012.

[16] D. Chirkin *et al.* *2019 15th International Conference on eScience (eScience)* (2019) 388–393.

[17] D. Chirkin. arXiv:1304.0735.

[18] **IceCube** Collaboration *PoS* **ICRC2019** (2021) 1031.

[19] F. Henningsen *et al.* *Journal of Instrumentation* **15** no. 07, (2020) P07031.

[20] F. Henningsen *et al.* *Journal of Instrumentation* **16** no. 09, (Sep, 2021) C09033.

PoS(ICRC2023)1034

Full Author List: IceCube Collaboration

R. Abbasi[17], M. Ackermann[63], J. Adams[18], S. K. Agarwalla[40, 64], J. A. Aguilar[12], M. Ahlers[22], J.M. Alameddine[23], N. M. Amin[44], K. Andeen[42], G. Anton[26], C. Argüelles[14], Y. Ashida[53], S. Athanasiadou[63], S. N. Axani[44], X. Bai[50], A. Balagopal V.[40], M. Baricevic[40], S. W. Barwick[30], V. Basu[40], R. Bay[8], J. J. Beatty[20, 21], J. Becker Tjus[11, 65], J. Beise[61], C. Bellenghi[27], C. Benning[1], S. BenZvi[52], D. Berley[19], E. Bernardini[48], D. Z. Besson[36], E. Blaufuss[19], S. Blot[63], F. Bontempo[31], J. Y. Book[14], C. Boscolo Meneguolo[48], S. Böser[41], O. Botner[61], J. Böttcher[1], E. Bourbeau[22], J. Braun[40], B. Brinson[6], J. Brostean-Kaiser[63], R. T. Burley[2], R. S. Busse[43], D. Butterfield[40], M. A. Campana[49], K. Carloni[14], E. G. Carnie-Bronca[2], S. Chattopadhyay[40, 64], N. Chau[12], C. Chen[6], Z. Chen[55], D. Chirkin[40], S. Choi[56], B. A. Clark[19], L. Classen[43], A. Coleman[61], G. H. Collin[15], A. Connolly[20, 21], J. M. Conrad[15], P. Coppin[13], P. Correa[13], D. F. Cowen[59, 60], P. Dave[6], C. De Clercq[13], J. J. DeLaunay[58], D. Delgado[14], S. Deng[1], K. Deoskar[54], A. Desai[40], P. Desiati[40], K. D. de Vries[13], G. de Wasseige[37], T. DeYoung[24], A. Diaz[15], J. C. Díaz-Vélez[40], M. Dittmer[43], A. Domi[26], H. Dujmovic[40], M. A. DuVernois[40], T. Ehrhardt[41], P. Eller[27], E. Ellinger[62], S. El Mentawi[1], D. Elsässer[23], R. Engel[31, 32], H. Erpenbeck[40], J. Evans[19], P. A. Evenson[44], K. L. Fan[19], K. Fang[40], K. Farrag[16], A. R. Fazely[7], A. Fedynitch[57], N. Feigl[10], S. Fiedlschuster[26], C. Finley[54], L. Fischer[63], D. Fox[59], A. Franckowiak[11], A. Fritz[41], P. Fürst[1], J. Gallagher[39], E. Ganster[1], A. Garcia[14], L. Gerhardt[9], A. Ghadimi[58], C. Glaser[61], T. Glauch[27], T. Glüsenkamp[26, 61], N. Goehlke[32], J. G. Gonzalez[44], S. Goswami[58], D. Grant[24], S. J. Gray[19], O. Gries[1], S. Griffin[40], S. Griswold[52], K. M. Groth[22], C. Günther[1], P. Gutjahr[23], C. Haack[26], A. Hallgren[61], R. Halliday[24], L. Halve[1], F. Halzen[40], H. Hamdaoui[55], M. Ha Minh[27], K. Hanson[40], J. Hardin[15], A. A. Harnisch[24], P. Hatch[33], A. Haungs[31], K. Helbing[62], J. Hellrung[11], F. Henningsen[27], L. Heuermann[1], N. Heyer[61], S. Hickford[62], A. Hidvegi[54], C. Hill[16], G. C. Hill[2], K. D. Hoffman[19], S. Hori[40], K. Hoshina[40, 66], W. Hou[31], T. Huber[31], K. Hultqvist[54], M. Hünnefeld[23], R. Hussain[40], K. Hymon[23], S. In[56], A. Ishihara[16], M. Jacquart[40], O. Janik[1], M. Jansson[54], G. S. Japaridze[5], M. Jeong[56], M. Jin[14], B. J. P. Jones[4], D. Kang[31], W. Kang[56], X. Kang[49], A. Kappes[43], D. Kappesser[41], L. Kardum[23], T. Karg[63], M. Karl[27], A. Karle[40], U. Katz[26], M. Kauer[40], J. L. Kelley[40], A. Khatee Zathul[40], A. Kheirandish[34, 35], J. Kiryluk[55], S. R. Klein[8, 9], A. Kochocki[24], R. Koirala[44], H. Kolanoski[10], T. Kontrimas[27], L. Köpke[41], C. Kopper[26], D. J. Koskinen[22], P. Koundal[31], M. Kovacevich[49], M. Kowalski[10, 63], T. Kozynets[22], J. Krishnamoorthi[40, 64], K. Kruiswijk[37], E. Krupczak[24], A. Kumar[63], E. Kun[11], N. Kurahashi[49], N. Lad[63], C. Lagunas Gualda[63], M. Lamoureux[37], M. J. Larson[19], S. Latseva[1], F. Lauber[62], J. P. Lazar[14, 40], J. W. Lee[56], K. Leonard DeHolton[60], A. Leszczyńska[44], M. Lincetto[11], Q. R. Liu[40], M. Liubarska[25], E. Lohfink[41], C. Love[49], C. J. Lozano Mariscal[43], L. Lu[40], F. Lucarelli[28], W. Luszczak[20, 21], Y. Lyu[8, 9], J. Madsen[40], K. B. M. Mahn[24], Y. Makino[40], E. Manao[27], S. Mancina[40, 48], W. Marie Sainte[40], I. C. Mariş[12], S. Marka[46], Z. Marka[46], M. Marsee[58], I. Martinez-Soler[14], R. Maruyama[45], F. Mayhew[24], T. McElroy[25], F. McNally[38], J. V. Mead[22], K. Meagher[40], S. Mechbal[63], A. Medina[21], M. Meier[16], Y. Merckx[13], L. Merten[11], J. Micallef[24], J. Mitchell[7], T. Montaruli[28], R. W. Moore[25], Y. Morii[16], R. Morse[40], M. Moulai[40], T. Mukherjee[31], R. Naab[63], R. Nagai[16], M. Nakos[40], U. Naumann[62], J. Necker[63], A. Negi[4], M. Neumann[43], H. Niederhausen[24], M. U. Nisa[24], A. Noell[1], A. Novikov[44], S. C. Nowicki[24], A. Obertacke Pollmann[16], V. O'Dell[40], M. Oehler[31], B. Oeyen[29], A. Olivas[19], R. Ørsøe[27], J. Osborn[40], E. O'Sullivan[61], H. Pandya[44], N. Park[33], G. K. Parker[4], E. N. Paudel[44], L. Paul[42, 50], C. Pérez de los Heros[61], J. Peterson[40], S. Philippen[1], A. Pizzuto[40], M. Plum[50], A. Pontén[61], Y. Popovych[41], M. Prado Rodriguez[40], B. Pries[24], R. Procter-Murphy[19], G. T. Przybylski[9], C. Raab[37], J. Rack-Helleis[41], K. Rawlins[3], Z. Rechav[40], A. Rehman[44], P. Reichherzer[11], G. Renzi[12], E. Resconi[27], S. Reusch[63], W. Rhode[23], B. Riedel[40], A. Rifaie[1], E. J. Roberts[2], S. Robertson[8, 9], S. Rodan[56], G. Roellinghoff[56], M. Rongen[26], C. Rott[53, 56], T. Ruhe[23], L. Ruohan[27], D. Ryckbosch[29], I. Safa[14, 40], J. Saffer[32], D. Salazar-Gallegos[24], P. Sampathkumar[31], S. E. Sanchez Herrera[24], A. Sandrock[62], M. Santander[58], S. Sarkar[25], S. Sarkar[47], J. Savelberg[1], P. Savina[40], M. Schaufel[1], H. Schieler[31], S. Schindler[26], L. Schlickmann[1], B. Schlüter[43], F. Schlüter[12], N. Schmeisser[62], T. Schmidt[19], J. Schneider[26], F. G. Schröder[31, 44], L. Schumacher[26], G. Schwefer[1], S. Sclafani[19], D. Seckel[44], M. Seikh[36], S. Seunarine[51], R. Shah[49], A. Sharma[61], S. Shefali[32], N. Shimizu[16], M. Silva[40], B. Skrzypek[14], B. Smithers[4], R. Snihur[40], J. Soedingrekso[23], A. Søgaard[22], D. Soldin[32], P. Soldin[1], G. Sommani[11], C. Spannfellner[27], G. M. Spiczak[51], C. Spiering[63], M. Stamatikos[21], T. Stanev[44], T. Stezelberger[9], T. Stürwald[62], T. Stuttard[22], G. W. Sullivan[19], I. Taboada[6], S. Ter-Antonyan[7], M. Thiesmeyer[1], W. G. Thompson[14], J. Thwaites[40], S. Tilav[44], K. Tollefson[24], C. Tönnis[56], S. Toscano[12], D. Tosi[40], A. Trettin[63], C. F. Tung[6], R. Turcotte[31], J. P. Twagirayezu[24], B. Ty[40], M. A. Unland Elorrieta[43], A. K. Upadhyay[40, 64], K. Upshaw[7], N. Valtonen-Mattila[61], J. Vandenbroucke[40], N. van Eijndhoven[13], D. Vannerom[15], J. van Santen[63], J. Vara[43], J. Veitch-Michaelis[40], M. Venugopal[31], M. Vereecken[37], S. Verpoest[44], D. Veske[46], A. Vijai[19], C. Walck[54], C. Weaver[24], P. Weigel[15], A. Weindl[31], J. Weldert[60], C. Wendt[40], J. Werthebach[23], M. Weyrauch[31], N. Whitehorn[24], C. H. Wiebusch[1], N. Willey[24], D. R. Williams[58], L. Witthaus[23], A. Wolf[1], M. Wolf[27], G. Wrede[26], X. W. Xu[7], J. P. Yanez[25], E. Yildizci[40], S. Yoshida[16], R. Young[36], F. Yu[14], S. Yu[24], T. Yuan[40], Z. Zhang[55], P. Zhelnin[14], M. Zimmerman[40]

[1] III. Physikalisches Institut, RWTH Aachen University, D-52056 Aachen, Germany
[2] Department of Physics, University of Adelaide, Adelaide, 5005, Australia
[3] Dept. of Physics and Astronomy, University of Alaska Anchorage, 3211 Providence Dr., Anchorage, AK 99508, USA
[4] Dept. of Physics, University of Texas at Arlington, 502 Yates St., Science Hall Rm 108, Box 19059, Arlington, TX 76019, USA
[5] CTSPS, Clark-Atlanta University, Atlanta, GA 30314, USA
[6] School of Physics and Center for Relativistic Astrophysics, Georgia Institute of Technology, Atlanta, GA 30332, USA
[7] Dept. of Physics, Southern University, Baton Rouge, LA 70813, USA
[8] Dept. of Physics, University of California, Berkeley, CA 94720, USA
[9] Lawrence Berkeley National Laboratory, Berkeley, CA 94720, USA
[10] Institut für Physik, Humboldt-Universität zu Berlin, D-12489 Berlin, Germany
[11] Fakultät für Physik & Astronomie, Ruhr-Universität Bochum, D-44780 Bochum, Germany
[12] Université Libre de Bruxelles, Science Faculty CP230, B-1050 Brussels, Belgium

PoS(ICRC2023)1034

[13] Vrije Universiteit Brussel (VUB), Dienst ELEM, B-1050 Brussels, Belgium
[14] Department of Physics and Laboratory for Particle Physics and Cosmology, Harvard University, Cambridge, MA 02138, USA
[15] Dept. of Physics, Massachusetts Institute of Technology, Cambridge, MA 02139, USA
[16] Dept. of Physics and The International Center for Hadron Astrophysics, Chiba University, Chiba 263-8522, Japan
[17] Department of Physics, Loyola University Chicago, Chicago, IL 60660, USA
[18] Dept. of Physics and Astronomy, University of Canterbury, Private Bag 4800, Christchurch, New Zealand
[19] Dept. of Physics, University of Maryland, College Park, MD 20742, USA
[20] Dept. of Astronomy, Ohio State University, Columbus, OH 43210, USA
[21] Dept. of Physics and Center for Cosmology and Astro-Particle Physics, Ohio State University, Columbus, OH 43210, USA
[22] Niels Bohr Institute, University of Copenhagen, DK-2100 Copenhagen, Denmark
[23] Dept. of Physics, TU Dortmund University, D-44221 Dortmund, Germany
[24] Dept. of Physics and Astronomy, Michigan State University, East Lansing, MI 48824, USA
[25] Dept. of Physics, University of Alberta, Edmonton, Alberta, Canada T6G 2E1
[26] Erlangen Centre for Astroparticle Physics, Friedrich-Alexander-Universität Erlangen-Nürnberg, D-91058 Erlangen, Germany
[27] Technical University of Munich, TUM School of Natural Sciences, Department of Physics, D-85748 Garching bei München, Germany
[28] Département de physique nucléaire et corpusculaire, Université de Genève, CH-1211 Genève, Switzerland
[29] Dept. of Physics and Astronomy, University of Gent, B-9000 Gent, Belgium
[30] Dept. of Physics and Astronomy, University of California, Irvine, CA 92697, USA
[31] Karlsruhe Institute of Technology, Institute for Astroparticle Physics, D-76021 Karlsruhe, Germany
[32] Karlsruhe Institute of Technology, Institute of Experimental Particle Physics, D-76021 Karlsruhe, Germany
[33] Dept. of Physics, Engineering Physics, and Astronomy, Queen's University, Kingston, ON K7L 3N6, Canada
[34] Department of Physics & Astronomy, University of Nevada, Las Vegas, NV, 89154, USA
[35] Nevada Center for Astrophysics, University of Nevada, Las Vegas, NV 89154, USA
[36] Dept. of Physics and Astronomy, University of Kansas, Lawrence, KS 66045, USA
[37] Centre for Cosmology, Particle Physics and Phenomenology - CP3, Université catholique de Louvain, Louvain-la-Neuve, Belgium
[38] Department of Physics, Mercer University, Macon, GA 31207-0001, USA
[39] Dept. of Astronomy, University of Wisconsin–Madison, Madison, WI 53706, USA
[40] Dept. of Physics and Wisconsin IceCube Particle Astrophysics Center, University of Wisconsin–Madison, Madison, WI 53706, USA
[41] Institute of Physics, University of Mainz, Staudinger Weg 7, D-55099 Mainz, Germany
[42] Department of Physics, Marquette University, Milwaukee, WI, 53201, USA
[43] Institut für Kernphysik, Westfälische Wilhelms-Universität Münster, D-48149 Münster, Germany
[44] Bartol Research Institute and Dept. of Physics and Astronomy, University of Delaware, Newark, DE 19716, USA
[45] Dept. of Physics, Yale University, New Haven, CT 06520, USA
[46] Columbia Astrophysics and Nevis Laboratories, Columbia University, New York, NY 10027, USA
[47] Dept. of Physics, University of Oxford, Parks Road, Oxford OX1 3PU, United Kingdom
[48] Dipartimento di Fisica e Astronomia Galileo Galilei, Università Degli Studi di Padova, 35122 Padova PD, Italy
[49] Dept. of Physics, Drexel University, 3141 Chestnut Street, Philadelphia, PA 19104, USA
[50] Physics Department, South Dakota School of Mines and Technology, Rapid City, SD 57701, USA
[51] Dept. of Physics, University of Wisconsin, River Falls, WI 54022, USA
[52] Dept. of Physics and Astronomy, University of Rochester, Rochester, NY 14627, USA
[53] Department of Physics and Astronomy, University of Utah, Salt Lake City, UT 84112, USA
[54] Oskar Klein Centre and Dept. of Physics, Stockholm University, SE-10691 Stockholm, Sweden
[55] Dept. of Physics and Astronomy, Stony Brook University, Stony Brook, NY 11794-3800, USA
[56] Dept. of Physics, Sungkyunkwan University, Suwon 16419, Korea
[57] Institute of Physics, Academia Sinica, Taipei, 11529, Taiwan
[58] Dept. of Physics and Astronomy, University of Alabama, Tuscaloosa, AL 35487, USA
[59] Dept. of Astronomy and Astrophysics, Pennsylvania State University, University Park, PA 16802, USA
[60] Dept. of Physics, Pennsylvania State University, University Park, PA 16802, USA
[61] Dept. of Physics and Astronomy, Uppsala University, Box 516, S-75120 Uppsala, Sweden
[62] Dept. of Physics, University of Wuppertal, D-42119 Wuppertal, Germany
[63] Deutsches Elektronen-Synchrotron DESY, Platanenallee 6, 15738 Zeuthen, Germany
[64] Institute of Physics, Sachivalaya Marg, Sainik School Post, Bhubaneswar 751005, India
[65] Department of Space, Earth and Environment, Chalmers University of Technology, 412 96 Gothenburg, Sweden
[66] Earthquake Research Institute, University of Tokyo, Bunkyo, Tokyo 113-0032, Japan

Acknowledgements

The authors gratefully acknowledge the support from the following agencies and institutions: USA – U.S. National Science Foundation-Office of Polar Programs, U.S. National Science Foundation-Physics Division, U.S. National Science Foundation-EPSCoR, Wisconsin Alumni Research Foundation, Center for High Throughput Computing (CHTC) at the University of Wisconsin–Madison, Open Science

PoS(ICRC2023)1034

Grid (OSG), Advanced Cyberinfrastructure Coordination Ecosystem: Services & Support (ACCESS), Frontera computing project at the Texas Advanced Computing Center, U.S. Department of Energy-National Energy Research Scientific Computing Center, Particle astrophysics research computing center at the University of Maryland, Institute for Cyber-Enabled Research at Michigan State University, and Astroparticle physics computational facility at Marquette University; Belgium – Funds for Scientific Research (FRS-FNRS and FWO), FWO Odysseus and Big Science programmes, and Belgian Federal Science Policy Office (Belspo); Germany – Bundesministerium für Bildung und Forschung (BMBF), Deutsche Forschungsgemeinschaft (DFG), Helmholtz Alliance for Astroparticle Physics (HAP), Initiative and Networking Fund of the Helmholtz Association, Deutsches Elektronen Synchrotron (DESY), and High Performance Computing cluster of the RWTH Aachen; Sweden – Swedish Research Council, Swedish Polar Research Secretariat, Swedish National Infrastructure for Computing (SNIC), and Knut and Alice Wallenberg Foundation; European Union – EGI Advanced Computing for research; Australia – Australian Research Council; Canada – Natural Sciences and Engineering Research Council of Canada, Calcul Québec, Compute Ontario, Canada Foundation for Innovation, WestGrid, and Compute Canada; Denmark – Villum Fonden, Carlsberg Foundation, and European Commission; New Zealand – Marsden Fund; Japan – Japan Society for Promotion of Science (JSPS) and Institute for Global Prominent Research (IGPR) of Chiba University; Korea – National Research Foundation of Korea (NRF); Switzerland – Swiss National Science Foundation (SNSF); United Kingdom – Department of Physics, University of Oxford.

PoS(ICRC2023)1034